Investigating the Eastern Alpine–Dinaric transition with teleseismic receiver functions: Evidence for subducted European Crust

Stefan Mroczek[a,b,*], Frederik Tilmann[a,b], Jan Pleuger[b], Xiaohui Yuan[a], Ben Heit[a], the SWATH-D Working Group[1], the AlpArray Working Group[2]

[a] *GFZ German Research Centre for Geosciences, Telegrafenberg, Potsdam, 14473, Brandenburg, Germany*
[b] *Freie Universitaet Berlin, Institute for Geological Sciences, Malteserstr. 74-100, Berlin, 12249, Germany*

Abstract

The tectonic structure of the Eastern Alps is heavily debated with successive geophysical studies unable to resolve areas of ambiguity (e.g., the presence of a switch in subduction polarity and differing crustal models). Here we produce a high resolution Moho map of the Eastern Alps based on a dense seismic broadband array deployment. Moho depths were derived from joint analysis of receiver function images of direct conversions and multiple reflections, which enables us to map overlapping discontinuities. We observe the European Moho to be underlying the Adriatic Moho from the west up to the eastern edge of the Tauern Window. East of this longitude, a sharp transition from underthrusting European to a flat and thinned crust associated with Pannonian extension tectonics occurs, which is underthrust by both European crust in the north and by Adriatic crust in the south. The northeast-directed underthrusting of Adriatic lithosphere deepens towards the east as it transitions to subduction below the northwestern Dinarides. Our results suggest that the steep high velocity region in the mantle below the Eastern Alps, observed in tomographic studies, is likely to be of European origin.

Keywords: Seismology, Moho map, Receiver functions, Alps

1. Introduction

Compared to oceanic subduction with a non-ambiguous sense of subduction and strongly localised deformation, continental convergence zones are characterized by wider deformation zones and interacting crustal blocks. This is especially true in the Eastern Alps where a

*Corresponding author
Email address: mroczek@gfz-potsdam.de (Stefan Mroczek)

[1]Members of the SWATH-D Working Group who are not otherwise co-authors are M. Weber and C. Haberland.

[2]The complete member list for the AlpArray Working group can be found at alparray.ethz.ch

stage of southward subduction of the Alpine Tethys was followed by collision of European and Adriatic continental lithosphere. During the final stages of orogeny, Eastern Alpine units escaped eastward into the opening Pannonian Basin (Ratschbacher et al., 1991) while at the same time the upper-plate Adriatic continental crust penetrated into the Alps.

Historically, the subduction of European lithosphere was assumed to be continuous across the entire Alps (e.g. Laubscher, 1970, 1971, 1975; Frisch, 1979), with the Adriatic microplate subducting in the east below the Dinarides (Laubscher, 1971). The subduction of European lithosphere has been confirmed with receiver function images of dipping Moho and Moho offsets in the Western and Central Alps (e.g. Lombardi et al., 2008; Spada et al., 2013; Zhao et al., 2015; Kummerow et al., 2004).

Teleseismic tomography results have consistently shown at least two main positive velocity anomalies in the upper mantle below the Alps (e.g. Babuška et al., 1990; Lippitsch et al., 2003; Piromallo and Morelli, 2003; Mitterbauer et al., 2011; Karousová et al., 2013; Zhao et al., 2016; Paffrath et al., 2021; Plomerová et al., 2022). The western anomaly is accepted to be of European origin while the eastern anomaly has, in some studies, an apparent northerly dip leading to debate about its origin, either being of Adriatic or mixed European and Adriatic, rather than purely European, provenance (Babuška et al., 1990; Lippitsch et al., 2003; Karousová et al., 2013; Handy et al., 2015; Plomerová et al., 2022). This idea implies there is a change in subduction direction, i.e., a polarity switch from European subduction towards the south (in the Western and Central Alps) to Adriatic subduction towards the north in the Eastern Alps (linked to the Adriatic subduction beneath the Dinarides). Numerous studies probed the nature and location of this hypothetical polarity switch and its geodynamic implications but have failed to provide conclusive results (e.g. Kissling et al., 2006; Ustaszewski et al., 2008; Handy et al., 2015). The TRANSALP profile (12°E), where a combination of passive (Kummerow et al., 2004) and controlled source (Lüschen et al., 2006) seismic imaging was employed, shows a gently southward dipping European Moho terminated by a jump to a shallow and sub-horizontal Adriatic Moho. The location of this transect is of particular interest because it falls almost exactly between the two main positive velocity anomalies described above.

The CELEBRATION 2000 (Guterch et al., 2003) and the ALP2002 (labelled ALP-01 and ALP-02 on Figure 1) controlled source seismic (CSS) experiments reveal a region where thinned Pannonian crust (to the east) and the European Moho (showing a clear southward dip) intersect with Adriatic Moho to the south, suggesting that Europe remains the underlying plate (Brückl et al., 2010, 2007; Behm et al., 2007).

The best data coverage is provided along the N-S profile at 13.3°E by the passive EASI transect (AlpArray Seismic Network, 2014) which crosses a gap in the Moho map of Spada et al. (2013). The receiver function study carried out by Hetényi et al. (2018b), using the EASI temporary stations (Figure 1) plus some permanent stations, showed the Adriatic and European Mohos forming a trough-like structure with a horizontal gap of nearly 50 km. They suggested that this gap does not contain a sharp Moho boundary but instead a ~20 km thick gradient zone reaching approximately 70 km depth. They connected this deeper gradient zone with the Adriatic Moho (making it consistent with Adriatic subduction) rather than with the European Moho.

An additional study probing the Moho and the mantle was conducted by Kind et al. (2021). Using stations that covered a much larger area, the method of stacking of S receiver functions without deconvolution was employed. This work not only mapped the Moho but also identified clear signals from negative velocity gradients in the mantle (NVGs), which have a dominant southern dip direction beneath the Alps. According to the authors, these interfaces (sometimes interpreted as the lithosphere-asthenosphere boundary (LAB)) seem to be distributed in the entire Alpine region and could be indicative of its tectonic history.

1.1. Outline of the tectonic evolution of the Eastern Alps

The Eastern and eastern Southern Alps are a bivergent orogen consisting of a pro-wedge built up of units that were thrust northward onto the European foreland and a retro-wedge built up of units thrust southward onto Adria. From top to bottom, the pro-wedge consists of the Austroalpine nappes, the Penninic units derived from the Late Jurassic-mid-Cretaceous Alpine Tethys including small pieces of continental crust from within this oceanic basin, and Subpenninic and Helvetic units derived from the former European continental margin (e.g. Froitzheim et al., 2008; Schuster et al., 2013). Mostly in the Cretaceous, the Austroalpine units were assembled from the upper and lower plate of a probably intracontinental subduction zone within Adria (Stüwe and Schuster, 2010). In this eo-Alpine orogen, most of the sedimentary cover of the Austroalpine units was sheared off and piled up in an external position, forming the present-day Northern Calcareous Alps, while the basement units that were subducted deepest are now exposed in the axial parts of the Eastern Alps. The Alpine Tethys was subducted below Adria probably from the Early Cretaceous onwards (Faupl and Tollmann, 1979). Its suturing in the Eocene was followed by subduction of the thinned distal European continental margin and Oligocene collision of thicker European crust with Adria (e.g. Kurz et al., 2008). The occurrence of Penninic and Subpenninic units in the Eastern Alps is limited to a few tectonic windows. The largest of them, situated in the centre of our study area, is the Tauern Window (TW, Figure 1) where Subpenninic units framed by Penninic ones are exposed below the Austroalpine units. In the Neogene, European subduction in the Eastern Alps largely ceased as indicated by Neogene shortening amounts along the Northern Alpine Front of only a few kilometers (Hinsch, 2013). Instead, further convergence between the European and Adriatic plates was mostly accommodated by underthrusting of Adriatic crust below the pro-wedge, backthrusting in the Southern Alpine retro-wedge, and lateral extrusion of the Eastern Alps into the Pannonian Basin (Frisch et al., 1998). Major structures that accommodated this lateral extrusion are the dextral Periadriatic Fault along the boundary of the Eastern and Southern Alps and the sinistral Inntal and Salzachtal-Ennstal-Mariazell-Puchberg (SEMP) faults farther north as well as the Brenner and Katschberg normal faults at the western and eastern border of the TW, respectively (e.g. Rosenberg and Schneider, 2008). In the northwestern external Dinarides, the underthrusting of Adria below the Dinaric carbonate platform caused several tens of kilometres of top-to-the-WSW shortening that were mostly accommodated in the Eocene, based on the age of syntectonic flysch. Further Neogene convergence between Adria and Europe was partitioned into south-vergent thrusts in the Southern Alps systematically overprinting older Dinaric structures (Doglioni, 1987), minor shortening along the

Dinaric frontal thrust on Istria peninsula, and a system of NW-SE striking dextral strike-slip faults between the Dinaric front and the Periadriatic Fault (Placer, 1998; Vrabec and Fodor, 2006). Neogene deformation in the evolving Pannonian basin was characterised by progressive younging from west to east of magmatism and the formation of depocentres (e.g. Csontos et al., 1992; Pecskay et al., 2006). This is commonly interpreted to reflect a separation of the European slab into an Alpine and a Carpathian segment along a tear (e.g. Mason et al., 1998) and enhanced rollback of the European slab in the Carpathians due to subduction of a landlocked remnant of the Alpine Tethys (Royden, 1993). This rollback led to strong extensional thinning of the crust and lithosphere below the Pannonian basin (e.g. Horváth et al., 2006), concomitant with breakoff of the slab propagating from west to east.

2. Data and Methodology

In order to improve the data coverage in the Eastern Alps, the large SWATH-D deployment (Heit et al., 2021) was operated within the AlpArray initiative. Here, we analyse data provided by the SWATH-D experiment which consisted of 163 broadband stations in a wide E-W oriented network configuration with a nominal interstation distance of 15 km (Figure 1). We exploited the dense coverage of the SWATH-D network as well as the concurrent AlpArray networks (Hetényi et al., 2018a) and the aforementioned EASI experiment to construct common conversion point (CCP) stacks (Kind et al., 2002) of receiver functions (RFs), which helped to constrain the 3-D layout of the crust, including subducted fragments of lithosphere in the study region (Figure 1).

We calculated RFs for the SV (S-wave vertical polarisation) and SH (S-wave horizontal polarisation) components from teleseismic P, PP, and PKP waveforms (see Kind and Yuan (2011) for a review and Sections S1 and S2 in the supplemental material for a more detailed description). The SV-RFs are standard tools for imaging horizontal interfaces, while SH-RFs are more sensitive to dipping structures. A subset of the used events and the back-azimuthal distribution for the full catalogue are plotted in Figure S1.

CCP stacks for both the SV and SH RFs were then assembled using a 1-D velocity model for the area (Jozi Najafabadi et al., 2021). In addition to CCP stacks for the primary conversion (Ps), we also calculated CCP stacks for the two main multiples (PpPs and PpSs+PsPs). For each cross section we show three CCP stacked images with the independent phases mentioned above (SV-Ps, SH-Ps, and SV-PpPs). As shown by synthetic tests (explained in detail in Section 3), each of the three phases has different sensitivities to horizontal or dipping interfaces.

We finally identify the Moho interfaces below these complex tectonic regions by combining all the CCP images with the guidance of the synthetic tests.

The Moho was picked manually, with the possibility of overlapping Moho conversions due to underthrusted or subduction crustal sections. For convenience we refer the European, Adriatic, and Pannonian Mohos in order to fit appropriate overlapping interfaces. Identification of, in particular southward, dipping interfaces is challenging on the SV-Ps CCP stacks as expected conversion amplitudes are small (see Section 3), therefore we also relied on the SH-Ps and SV-PpPs stacks to identify those interfaces. To make a pick on the dipping

sections of Moho, we required that it be visible on either the SV or SH component plus at least one of the multiples. For example, at 13.3°E and 14°E (Figures 2 and 3) the energy on the SV component continues to depths greater than 150 km, however, we only pick to the extent observed on the first multiple. These picks were then automatically re-picked and splines were fitted (with some manual adjustment) to obtain the Moho depth map. The spline coefficients, having been determined in the time domain, have units of Ps lag time and thus can be converted to splines for the first and second multiple with an appropriate Vp/Vs ratio. By maximising the fit of the spline with the multiple migrations, the average crustal Vp/Vs ratio was also determined. The normal CCP stacking procedure is based on a horizontally layered model, and will lead to artifacts when applied to phases converted at dipping interfaces (Cassidy, 1992), causing Vp/Vs to be overestimated and depth and dip to be underestimated. To account for this (to first order), we apply a dip-correction to the depths observed in the CCP stacks. For full details see Section S2.

3. Synthetic migration tests

The Moho geometry from different tectonic units beneath the study area is complex, with overlapping interfaces, horizontal, and strongly dipping segments present. As the event distribution is highly uneven (Figure S1), each of the RF phases/components has different sensitivities. Here we use synthetic RFs to evaluate the ability of different RF phases in recovering complicated Moho geometries. The target of the synthetic modelling is not to match the actual CCP stacks, but to provide clues about typical imaging artefacts and to test the capacity of our method to reconstruct the anomalies observed. In particular, we attempt to understand the role back azimuthal distribution might play in the fidelity of dipping structures in the images obtained. We calculated synthetic migrations using the full wavefield finite difference method of Roecker et al. (2010) with a bandwidth of 1.25 s to 100 s. The deconvolution was performed with a fixed water level of 10%, and the CCP stacking was carried out assuming the IASP91 velocity model. Vp was set to 6.1 km/s for the crust and 8 km/s for the mantle with Vs set according to a constant Vp/Vs=1.8). Synthetics were calculated for a range of models with geometry simplified from the main interfaces we observe in the actual CCP images. The synthetics were computed in 2-D with oblique incidence angles (2.5-D). The synthetics represent the upper limit of resolvability for the Moho in the Alps for receiver functions with densely spaced stations (15 km inter-station distance), high signal-to-noise ratios, no intracrustal interfaces, and a two-layer (crust and upper mantle) velocity model. Thus the limitations in imaging stem largely from the irregular distribution of teleseismic events. To approximate the true event back azimuth and slowness distribution while keeping the computational load moderate, we clustered the incidence angles and back-azimuths on a unit sphere (Banerjee et al., 2005). Incidence angles were calculated for a point approximately in the centre of the region of interest with mantle velocities. Synthetics were calculated using the mean back azimuth and slowness of each of the seven clusters (selected using the Bayesian Information Criterion after Schwarz, 1978). The events within each cluster can be assumed to have a high degree of waveform similarity. For the migration of the synthetic receiver functions, each synthetic waveform was weighted

by the total number of events originally in that cluster.

As mentioned, we consider the synthetics to represent the upper limit of our method to properly resolve the Moho. However, one aspect where the CCP stack of real data is likely to do better than synthetics is with respect to diffractions. In the real Earth case, diffractions are expected to be much weaker, as the velocity variations and the interface geometries are not as sharp as in the synthetic models and they also vary in 3-D rather than simply in 2-D (Lekić and Fischer, 2017). Thus, artefacts related to diffraction are likely exaggerated on the synthetic tests. Comparing the results of the tests with our actual observations (Figure 4), we observe some energy of Moho converted phases from the moderately dipping Moho on both the SV and SH components at 13.3°E (Figure 2, north of 46.5°N). Further east, at 14°E (Figure 3) we do not observe any energy from deep European Moho on the SV component below the flat section of the Pannonian Moho (south of 47.5°N). At first sight, this observation suggests the absence of subducted crust there. However, according to the synthetics shown in Figure 4, no coherent energy would be expected on the SV component for this southward-directed dip angle. This is induced by the majority of event back azimuths being from the N-E direction (Figure S1, so, for a more strongly southward dipping converter, incidence angles will be close to perpendicular and thus conversion coefficients will be very low. Therefore, we cannot conclude either for or against the presence of southward dipping European crust below the Pannonian Moho from the primary conversion (Ps phase) alone.

The event distribution should render a northerly dipping feature (such as the Adriatic Moho) easy to image due to high incidence angles resulting in large conversion coefficients such as at 14°E for the Adriatic Moho (Figure 4). In contrast, a southward dipping European Moho would be very difficult to image (on the SV component) due to the almost complete lack of back azimuths from the south. The situation is less ambiguous for multiples; for our northerly dominant back azimuth distribution, the conversion coefficient for the multiple phases for a southward dipping converter would be higher than for the Ps phase (Figure 4) and indeed we do observe a southward dipping European Moho for the first multiple (Figure 3).

4. Results and Discussion

Key CCP profiles are shown in Figure 2 (N-S profile through Tauern window), Figure 3 (N-S profile just east of the Tauern window) and Figure 5 (E-W profile). Figures 6 and 7 compare the N-S profiles with relevant synthetics and highlight the inferred Moho geometry corrected for dip. A larger suite of profiles can be found in the supplementary Section S5, Figures S10-S16. The Moho map is plotted in Figure 8. As demonstrated by the synthetic migrations (Section 3), we expect interfaces dipping towards the south to be difficult to image while those dipping towards the north will be more dominant.

4.1. Moho Geometry

In the west of the study area (up to 13°E), our results do not differ significantly from previous studies. The NFP-20 East CSS survey (Valasek et al., 1991, see Figure 1 for location) shows similar results to the section at 10°E (Figure S10). At 12°E, our results

agree well with those provided by the TRANSALP experiment (Kummerow et al., 2004) (Figure S12).

Our synthetic modelling (Figure 4) demonstrates that, given a realistic teleseismic event distribution, a simple Moho trough model with no sense of subduction could give rise to an apparent preference for northward subduction due to the stronger conversions for a north dipping interface, illuminated from predominantly northerly azimuths (Figure 6). For the European Moho alone there is little disagreement with Hetényi et al. (2018b) down to ~60 km depth. We go on to interpret deeper energy to be from the European Moho, based on the SH component and multiples. In contrast, in our interpretation the Adriatic Moho terminates much earlier, at approximately 40 km depth, similar to the Moho geometry of Spada et al. (2013).

4.2. Transition to the Pannonian region

The transect at 14.0°E (Figure 7) shows a distinctly different crustal structure from those to the west. A flat Moho at ~35 km depth between 47.5°N and 46.5°N is underthrusted by the European Moho from the north and by the Adriatic Moho from the south. This section of crust has presumably been thinned and reshaped during lateral extrusion into the Pannonian Basin (Ratschbacher et al., 1991), with possible additional removal of crust by delamination, which would imply the interface represents a new Moho. For convenience, we refer to this interface as Pannonian Moho, although its original provenance is Adriatic.

This thinned crust has been observed previously in the Eastern Alps by Brückl et al. (2010). With the CSS data from the ALP2002 experiment, Brückl et al. (2007) suggested a westward termination of the Pannonian Moho at approximately 14°E and then further refined this to ~13.6°E with 2-D elastic plate modelling (Brückl et al., 2010), approximately at the longitude of the eastern edge of the Tauern Window. We find the westward termination of the flat Moho section to be close to the point inferred by Brückl et al. (2010) (approximately 13.5°E visible on the E-W profile at 47.0°N- Figure 5), which is imaged directly in the CSS data of the E-W *ALP '75* profile (Yan and Mechie, 1989). The interpretation of this interface as being the Moho is confirmed by the ambient noise surface wave tomography of Lu et al. (2020), where it coincides with the 4.2 km/s Moho contour (shown by a dotted line on Figure 7), implying typical mantle velocities below. The western most extent of the thinned crust also coincides with a sharp increase in gravity moving eastwards out of the Tauern Window (Zahorec et al., 2021).

The visually step-like structure between the European and Pannonian Mohos coincides spatially with the SEMP fault, which marks the northerly extent of the lateral eastward extrusion of the Eastern Alps into the Pannonian Basin (Ratschbacher et al., 1991). A similar observation, using CSS data, was made further east across the Carpathian Arc where the dipping Moho interface from the European platform intersects the flat Moho below the Pannonian Basin (Tomek and Hall, 1993; Bielik et al., 2004).

Below the European to Pannonian Moho step, we image a sharply dipping interface that can be seen clearly on the SH component and the SV multiples. We interpret this interface as being continuous with the European Moho at least until 13.5°E (moving eastwards) and the onset of the Pannonian Moho. There is a small gap at 60 km depth between that and

the flat European Moho we observe on the SV component at 14°E. This gap is perhaps real or may be an artefact produced by a rather low conversion coefficient (the conversion coefficient depends on the angle of incidence). We choose to draw a connected interface based on continuity with migrations to the west but distinguish this as a region of high uncertainty.

Ongoing Adriatic subduction, with little shortening after the Oligocene, forms the Dinarides (Sun et al., 2019) to the south of our study area. As we move east from the flat Adriatic Moho we observe in the west, this transition must be reflected in the Moho geometry. By 14°E, the Adriatic Moho retreats and begins to dip below the Pannonian Moho. We observe the Adriatic Moho reaching the Pannonian Moho at 46.25°N at approximately 20 km greater depth (Figure 7). The Adriatic Moho may also underthrust the Pannonian Moho but only on the order of a few kilometers. We have high confidence in this observation as northerly back azimuths give high conversion coefficients (as demonstrated in the synthetic tests in Figure 4).

5. Comparison with teleseismic tomography

The two latest teleseismic tomography studies of Paffrath et al. (2021) and Plomerová et al. (2022) draw two different pictures of subduction in the Eastern Alps (Figure 9). Paffrath et al. (2021) find the eastern positive velocity anomaly in the upper mantle to have no connection to the overlying crust and interpret it to be detached European lithosphere (Handy et al., 2021). In contrast, Plomerová et al. (2022) observe two mantle positive anomalies. The first, corresponding to the eastern anomaly of Paffrath et al. (2021), connects to Adriatic crust and is interpreted to be of mixed European and Adriatic origin. Further north, a second anomaly is observed and interpreted to be consisting of European lithosphere. We focus here on the transect at 14°E which exemplifies the differences (Figure 9).

In the tomographic picture of Plomerová et al. (2022), the geometry of the Adriatic Moho would fit quite well if one were to draw a continuous line into the anomaly following the 4% velocity contour. This Moho geometry would support the interpretation of Hetényi et al. (2018b) at 13.3°E where the Adriatic Moho plunges below the European Moho. While the agreement is good at 14°E on the SV component, this interpretation is not supported with our data at 13.3°E (Figure 6). It is also at odds with the south dipping interface we observe on the SH component (Figure 7) which cuts the anomaly. A northward dipping Moho-like interface would be negative on the SH component (as opposed to red for southward dipping).

A fully detached slab as in Paffrath et al. (2021) and Handy et al. (2021), also agrees well with the SV component receiver functions, however the strong negative velocity anomaly above the slab is cut by the interface we observe on the SH component and multiple migrations. In Figures S17-S19, we compare the tomographic model of Paffrath et al. (2021) and our observations along our main transects.

The tomography is heavily influenced by the crustal corrections which can likely explain the differences between the two studies (Plomerová et al., 2022). This is even more important in trying to determine if there is a connection between the anomaly at depth and the crust. An overestimation of crustal velocity would necessitate a corresponding underestimation of

velocity at depth, potentially making an anomaly appear detached. The opposite could also be true, i.e. an underestimate of crustal velocities making a slab appear attached. Additionally, receiver functions image velocity contrasts so a layer well below the resolution limit of the tomography could still produce a clear conversion. Given these subtleties, we believe that an interface connecting the anomaly at depth with European crust cannot be ruled out based on teleseismic travel time tomography alone.

Only considering evidence from the receiver functions, the simplest explanation is a steeply southward dipping interface. This is additionally supported by the negative velocity gradients (NVGs) observed by Kind et al. (2021). The NVG at 14°E almost exactly follows Moho interface we trace before depth correction, thus we would expect a similar degree of depth correction for both.

Simply by maintaining a constant thickness, the layer formed between the Moho and the NVG could physically lead into the "consensus" slab where both studies agree that there is a positive velocity anomaly (Figure 9).

6. Tectonic Implications

West of 13.5°E, the Moho geometries described before (Section 4.1) are well in line with the classical tectonic concept of the Alps consisting of a pro-wedge and a retro-wedge underlain by European and Adriatic Moho, respectively. Farther east, the Moho configuration imaged in Figure 3 requires that lower crust is still attached to the downgoing European and Adriatic plates while the former upper crust sheared off from these plates overlies the Pannonian Moho (Figure 10c). Since the European and Adriatic Mohos dip below the Pannonian one, the undetached lower crust of both plates must be separated from the Pannonian Moho by intervening mantle material. We hypothesise that emplacement of the mantle material was the combined effect of a retreat of the Alpine segment of the European slab with respect to the Adriatic upper plate and rollback of the Carpathian segment of the European slab that caused strong thinning of the Alpine crust in the upper plate. Retreat of the European slab below the Alps may have already started when the Alpine Tethys was sutured or soon thereafter (Figure 10a), similar to scenarios proposed by Malusà et al. (2011) and Kissling and Schlunegger (2018) for the Western and Central Alps. In accordance with classical models of Alpine nappe formation (e.g. Schmid et al., 1996), we assume that the Subpenninic nappes were successively stacked upon each other along in-sequence thrusts but that, different from classical models, mantle material migrated along the décollement between the rear parts of the Subpenninic nappes and the subducting, non-detached European lower crust. The emplacement of mantle material below Penninic and Subpenninic nappes of the Alpine pro-wedge probably started when the Alpine Tethys and lithosphere comprising only thin crust of the former distal European passive margin were subducted. At this stage (~32 Ma, Figure 10a), asthenosphere upwelling above the European slab would be a potential cause of magmatism along the Periadriatic Fault. We assume that the northward advance of the Pannonian Moho was concomitant with steepening of the European slab because after suturing of the Alpine Tethys in the Eocene, the Northern Alpine Front hardly moved towards the foreland and became almost inactive in the Neogene. At 14°E,

the length of European Moho underthrust below the Alps far exceeds estimates of Neogene thrusting along the Northern Alpine Front and must have been subducted in pre-Neogene times. Together with steepening of the European slab, we consider eastward escape of Eastern Alpine orogenic crust into the Pannonian basin from the Miocene on as the main driver behind the formation of the Pannonian Moho. Considering values of 28%-39% and 47% for Miocene N-S directed shortening and E-W directed extension, respectively, in the Eastern Alps (Linzer et al., 2002), the eastward escape thinned the crust in the axial part of the Alps more efficiently than north-south convergence between Europe and Adria could have thickened it. We note that according to several authors, the Adriatic lower crust had started to underthrust below the evolving Southern Alps, causing N-S shortening also in the Eastern Alps in the Late Oligocene-Early Miocene (Schmid et al., 2013), before the Alps were affected by Carpathian rollback since the Early to Middle Miocene (Wölfler et al., 2011; Schmid et al., 2013). Irrespective of the relative timing of Adriatic underthrusting and Carpathian rollback, the presence of a flat Moho from below the eastern Tauern Window connecting seamlessly eastwards into the Moho below the Pannonian basin supports the notion that the flat Pannonian Moho was mostly shaped in conjunction with Carpathian rollback. Our finding that the European Moho below the Eastern Alps extends below the northern edge of the Adriatic Moho limits the amount of Neogene Adriatic underthrusting below the Alps to a few tens of kilometres. We consider this as evidence that no subduction polarity switch and, contrary to the Carpathian European slab segment, also no slab breakoff occurred below the Eastern Alps in the Neogene. According to our Moho map (Figure 8), the underthrust Adriatic Moho below the Eastern Alps directly continues into the Adriatic Moho below the Dinarides. In Figure 10, we assume that Late Oligocene-Early Miocene thrusting in the Southern Alps led to thickening of the Adriatic crust between the Dinaric Frontal Thrust and the Periadriatic Fault and that this crust was thinned again by transtensional faulting in the same area (Vrabec and Fodor, 2006). A system of dextral strike-slip faults in the external Dinarides, that roughly parallel the Dinaric Frontal Thrust and that are partly still active today, coincides with the southwestern limit of the Pannonian Moho below the Dinarides.

7. Conclusions

The SWATH-D and AlpArray seismic networks have allowed the Moho in the Eastern Alps to be delineated to an unprecedented degree of resolution. We are able to shed light on crustal configuration and produce a map of the Moho depth of this region in the Eastern Alps, in some place distiguishing overlapping Mohos. The Moho map, determined from receiver functions, shows a thinned Pannonian (originally Adriatic) crust east of the Tauern Window. At this longitude (14°E), a step from the Adriatic Moho to the Pannonian Moho suggests underthrusting, but only on the order of a few kilometers, while the European Moho dips steeply beneath the Pannonian Moho down to a depth of at least 150 km depth. We find no evidence for northward directed subduction of Adriatic lithosphere at this point. Moving west, the deeper subducted European crust shallows out to ~70 km depth by 12°E (TRANSALP), remaining the lower plate but now underthrusting directly beneath

the shallowly dipping Adriatic Moho.

Acknowledgments

We thank György Hetényi and Rainer Kind for discussions and valuable feedback as well as the AlpArray-EASI Working Group for their work on the EASI experiment and the AlpArray Working Group on the AlpArray Seismic Network. We would also like to extend our thanks to the Deutsche Forschungsgemeinschaft [Grant numbers TI-316/8-1, TI-316/601, YU 115/11-1, and PL 534/4-1] for the funding of this research. We thank Steven Roecker for making available his software WT_MPI used for synthetics calculation (Roecker et al., 2010).

We acknowledge and thank the SWATH-D Field Team (the complete list can be found at at doi:10.14470/MF7562601148) for the data collection).

8. Data and resources

Seismic data used for this publication are hosted at the GEOFON data centre (SWATH-D) and other data centres within EIDA (AlpArray data and permanent stations), see Section S4 for a full list of data references and network codes. The Moho map, equivalent Ps lag time map for the Moho conversion, and map of implied Vp/Vs are made available at https://nextcloud.gfz-potsdam.de/s/zB5dPNby6X2Kjnj (temporary link while under review). The hill shade map was calculated from the Copernicus EU-DEM (produced with funding by the European Union, doi:10.5270/ESA-c5d3d65).

References

AlpArray Seismic Network, 2014. Eastern Alpine Seismic Investigation (EASI) - AlpArray Complimentary Experiment doi:10.12686/ALPARRAY/XT_2014.

Babuška, V., Plomerova, J., Granet, M., 1990. The deep lithosphere in the Alps: a model inferred from P residuals. Tectonophysics 176, 137–165. doi:10.1016/0040-1951(90)90263-8.

Banerjee, A., Dhillon, I.S., Ghosh, J., Sra, S., Ridgeway, G., 2005. Clustering on the Unit Hypersphere using von Mises-Fisher Distributions. J. Mach. Learn. Res. 6.

Behm, M., Brückl, E., Chwatal, W., Thybo, H., 2007. Application of stacking and inversion techniques to three-dimensional wide-angle reflection and refraction seismic data of the Eastern Alps. Geophys. J. Int. 170, 275–298. doi:10.1111/j.1365-246X.2007.03393.x.

Bielik, M., Šefara, J., Kováč, M., Bezák, V., Plašienka, D., 2004. The Western Carpathians–interaction of Hercynian and Alpine processes. Tectonophysics 393, 63–86. doi:10.1016/j.tecto.2004.07.044.

Brückl, E., Behm, M., Decker, K., Grad, M., Guterch, A., Keller, G., Thybo, H., 2010. Crustal structure and active tectonics in the Eastern Alps. Tectonics 29. doi:10.1029/2009TC002491.

Brückl, E., Bleibinhaus, F., Gosar, A., Grad, M., Guterch, A., Hrubcová, P., Keller, G.R., Majdański, M., Šumanovac, F., Tiira, T., et al., 2007. Crustal structure due to collisional and escape tectonics in the Eastern Alps region based on profiles Alp01 and Alp02 from the ALP 2002 seismic experiment. J. Geophys. Res. 112. doi:10.1029/2006JB004687.

Cassidy, J., 1992. Numerical experiments in broadband receiver function analysis. Bull. Seismol. Soc. Am. 82, 1453–1474.

Crameri, F., 2021. Scientific colour maps. doi:10.5281/zenodo.5501399.

Csontos, L., Nagymarosy, A., Horváth, F., Kovac, M., 1992. Tertiary evolution of the Intra-Carpathian area: A model. Tectonophysics 208, 221–241. doi:10.1016/0040-1951(92)90346-8.

Doglioni, C., 1987. Tectonics of the Dolomites (Southern Alps, Northern Italy). J. Struct. Geol. 9, 181–193. doi:10.1016/0191-8141(87)90024-1.

Faupl, P., Tollmann, A., 1979. Die Roßfeldschichten: Ein Beispiel für Sedimentation im Bereich einer tektonisch aktiven Tiefseerinne aus der kalkalpinen Unterkreide. Geologische Rundschau 68, 93–120. doi:10.1007/BF01821124.

Frisch, W., 1979. Tectonic progradation and plate tectonic evolution of the Alps. Tectonophysics 60, 121–139.

Frisch, W., Kuhlemann, J., Dunkl, I., Brügel, A., 1998. Palinspastic reconstruction and topographic evolution of the Eastern Alps during late Tertiary tectonic extrusion. Tectonophysics 297, 1–15. doi:10.1016/S0040-1951(98)00160-7.

Froitzheim, N., Plašienka, D., Schuster, R., 2008. Alpine tectonics of the Alps and Western Carpathians, in: The Geology of Central Europe Volume 2: Mesozoic and Cenozoic. Geological Society of London. doi:10.1144/CEV2P.6.

Guterch, A., Grad, M., Keller, G., Posgay, K., Vozár, J., Špičák, A., Brückl, E., Hajnal, Z., Thybo, H., Selvi, O., et al., 2003. Celebration 2000 seismic experiment. Studia Geophysica et Geodaetica 47, 659–669.

Handy, M.R., Giese, J., Schmid, S.M., Pleuger, J., Spakman, W., Onuzi, K., Ustaszewski, K., 2019. Coupled crust-mantle response to slab tearing, bending, and rollback along the Dinaride-Hellenide orogen. Tectonics 38, 2803–2828. doi:10.1029/2019TC005524.

Handy, M.R., Schmid, S.M., Paffrath, M., Friederich, W., the AlpArray Working Group, 2021. Orogenic lithosphere and slabs in the greater Alpine area – interpretations based on teleseismic P-wave tomography. Solid Earth 12, 2633–2669. doi:10.5194/se-12-2633-2021.

Handy, M.R., Ustaszewski, K., Kissling, E., 2015. Reconstructing the Alps–Carpathians–Dinarides as a key to understanding switches in subduction polarity, slab gaps and surface motion. Int. J. Earth Sci. 104, 1–26. doi:10.1007/s00531-014-1060-3.

Heit, B., Cristiano, L., Haberland, C., Tilmann, F., Pesaresi, D., Jia, Y., Hausmann, H., Hemmleb, S., Haxter, M., Zieke, T., Jaeckl, K., Schloemer, A., Weber, M., 2021. The SWATH-D Seismological Network in the Eastern Alps. Seismol. Res. Lett. 92, 1592–1609. doi:10.1785/0220200377.

Hetényi, G., Molinari, I., Clinton, J., Bokelmann, G., Bondár, I., Crawford, W.C., Dessa, J.X., Doubre, C., Friederich, W., Fuchs, F., et al., 2018a. The AlpArray Seismic Network: A large-scale European experiment to image the Alpine orogen. Surv. Geophys. doi:10.1007/s10712-018-9472-4.

Hetényi, G., Plomerová, J., Bianchi, I., Exnerová, H.K., Bokelmann, G., Handy, M.R., Babuška, V., AlpArray-EASI Working Group and others, 2018b. From mountain summits to roots: Crustal structure of the Eastern Alps and Bohemian Massif along longitude 13.3°E. Tectonophysics 744, 239–255. doi:10.1016/j.tecto.2018.07.001.

Hinsch, R., 2013. Laterally varying structure and kinematics of the Molasse fold and thrust belt of the Central Eastern Alps: Implications for exploration. AAPG Bulletin 97, 1805–1831. doi:10.1306/04081312129.

Horváth, F., Bada, G., Szafián, P., Tari, G., Ádám, A., Cloetingh, S., 2006. Formation and deformation of the Pannonian Basin: constraints from observational data. Geological Society, London, Memoirs 32, 191–206. doi:10.1144/GSL.MEM.2006.032.01.11.

Jozi Najafabadi, A., Haberland, C., Ryberg, T., Verwater, V.F., Le Breton, E., Handy, M.R., Weber, M., the AlpArray and AlpArray SWATH-D working groups, 2021. Relocation of earthquakes in the southern and eastern Alps (Austria, Italy) recorded by the dense, temporary SWATH-D network using a Markov chain Monte Carlo inversion. Solid Earth 12, 1087–1109. doi:10.5194/se-12-1087-2021.

Karousová, H., Plomerová, J., Babuška, V., 2013. Upper-mantle structure beneath the southern Bohemian Massif and its surroundings imaged by high-resolution tomography. Geophys. J. Int. 194, 1203–1215.

Kind, R., Schmid, S.M., Yuan, X., Heit, B., Meier, T., the AlpArray, Groups, A.S.D.W., 2021. Moho and uppermost mantle structure in the Alpine area from S-to-P converted waves. Solid Earth 12, 2503–2521. doi:10.5194/se-12-2503-2021.

Kind, R., Yuan, X., 2011. Seismic receiver function technique, in: Gupta, H. (Ed.), Encyclopedia of Solid Earth Geophysics. Springer, pp. 1258–1269. doi:10.1007/978-90-481-8702-7_12.

Kind, R., Yuan, X., Saul, J., Nelson, D., Sobolev, S., Mechie, J., Zhao, W., Kosarev, G., Ni, J., Achauer, U., et al., 2002. Seismic images of crust and upper mantle beneath Tibet: Evidence for Eurasian Plate subduction. Science 298, 1219–1221.

Kissling, E., Schlunegger, F., 2018. Rollback Orogeny Model for the Evolution of the Swiss Alps. Tectonics 37, 1097–1115. doi:10.1002/2017TC004762.

Kissling, E., Schmid, S.M., Lippitsch, R., Ansorge, J., Fügenschuh, B., 2006. Lithosphere structure and tectonic evolution of the Alpine arc: new evidence from high-resolution teleseismic tomography. Geological Society, London, Memoirs 32, 129–145. doi:10.1144/GSL.MEM.2006.032.01.08.

Kummerow, J., Kind, R., Oncken, O., Giese, P., Ryberg, T., Wylegalla, K., Scherbaum, F., Group, T.W., et al., 2004. A natural and controlled source seismic profile through the Eastern Alps: TRANSALP. Earth Planet. Sci. Lett. 225, 115–129. doi:10.1016/j.epsl.2004.05.040.

Kurz, W., Handler, R., Bertoldi, C., 2008. Tracing the exhumation of the eclogite zone (tauern window, eastern alps) by 40Ar/39Ar dating of white mica in eclogites, in: Orogenic Processes in the Alpine Collision Zone. Springer, pp. S191–S206.

Laubscher, H., 1970. Bewegung und Wärme in der alpinen Orogenese. Schweizerische mineralogische und petrographische Mitteilungen 50, 565–596.

Laubscher, H., 1971. Das Alpen-Dinariden-Problem und die Palinspastik der südlichen Tethys. Geologische rundschau 60, 813–833. doi:10.1007/BF02046522.

Laubscher, H.P., 1975. Plate boundaries and microplates in Alpine history. Am. J. Sci. 275, 865–876. doi:10.2475/ajs.275.8.865.

Lekić, V., Fischer, K.M., 2017. Interpreting spatially stacked Sp receiver functions. Geophys. J. Int. 210, 874–886. doi:10.1093/gji/ggx206.

Linzer, H.G., Decker, K., Peresson, H., Dell'Mour, R., Frisch, W., 2002. Balancing lateral orogenic float of the eastern alps. Tectonophysics 354, 211–237. doi:10.1016/S0040-1951(02)00337-2.

Lippitsch, R., Kissling, E., Ansorge, J., 2003. Upper mantle structure beneath the Alpine orogen from high-resolution teleseismic tomography. J. Geophys. Res. 108. doi:10.1029/2002JB002016.

Lombardi, D., Braunmiller, J., Kissling, E., Giardini, D., 2008. Moho depth and Poisson's ratio in the Western-Central Alps from receiver functions. Geophys. J. Int. 173, 249–264.

Lu, Y., Stehly, L., Brossier, R., Paul, A., AlpArray Working Group, 2020. Imaging Alpine crust using ambient noise wave-equation tomography. Geophys. J. Int. 222, 69–85. doi:10.1093/gji/ggaa145.

Lüschen, E., Borrini, D., Gebrande, H., Lammerer, B., Millahn, K., Neubauer, F., Nicolich, R., Group, T.W., et al., 2006. TRANSALP—deep crustal Vibroseis and explosive seismic profiling in the Eastern Alps. Tectonophysics 414, 9–38. doi:10.1016/j.tecto.2005.10.014.

Malusà, M.G., Faccenna, C., Garzanti, E., Polino, R., 2011. Divergence in subduction zones and exhumation of high pressure rocks (eocene western alps). Earth Planet. Sci. Lett. 310, 21–32. doi:10.1016/j.epsl.2011.08.002.

Mason, P.R., Seghedi, I., Szákacs, A., Downes, H., 1998. Magmatic constraints on geodynamic models of subduction in the East Carpathians, Romania. Tectonophysics 297, 157–176. doi:10.1016/S0040-1951(98)00167-X.

Mitterbauer, U., Behm, M., Brückl, E., Lippitsch, R., Guterch, A., Keller, G.R., Koslovskaya, E., Rumpfhuber, E.M., Šumanovac, F., 2011. Shape and origin of the East-Alpine slab constrained by the ALPASS teleseismic model. Tectonophysics 510, 195–206. doi:10.1016/j.tecto.2011.07.001.

Paffrath, M., Friederich, W., the AlpArray and AlpArray-Swath D working group, 2021. Imaging structure and geometry of slabs in the greater Alpine area – A P-wave traveltime tomography using AlpArray Seismic Network data. Solid Earth Discussions 2021, 1–40. doi:10.5194/se-2021-58.

Pecskay, Z., Lexa, J., Szakacs, A., Seghedi, I., Balogh, K., Konecny, V., Zelenka, T., Kovacs, M., Poka, T., Fulop, A., et al., 2006. Geochronology of Neogene magmatism in the Carpathian arc and intra-Carpathian area. Geologica Carpathica 57, 511.

Piromallo, C., Morelli, A., 2003. P wave tomography of the mantle under the Alpine-Mediterranean area. J. Geophys. Res. 108.

Placer, L., 1998. Contribution to the macrotectonic subdivision of the border region between Southern Alps

and External Dinarides. Geologija 41, 223?255. doi:10.5474/geologija.1998.013.

Plomerová, J., Žlebčíková, H., Hetényi, G., Vecsey, L., Babuška, V., AlpArray-EASI, working groups, A., 2022. Two subduction-related heterogeneities beneath the Eastern Alps and the Bohemian Massif imaged by high-resolution P-wave tomography. Solid Earth 13, 251–270. doi:10.5194/se-13-251-2022.

Ratschbacher, L., Frisch, W., Linzer, H.G., Merle, O., 1991. Lateral extrusion in the Eastern Alps, part 2: Structural analysis. Tectonics 10, 257–271. doi:10.1029/90TC02623.

Roecker, S., Baker, B., McLaughlin, J., 2010. A finite-difference algorithm for full waveform teleseismic tomography. Geophys. J. Int. 181, 1017–1040. doi:10.1111/j.1365-246X.2010.04553.x.

Rosenberg, C.L., Schneider, S., 2008. The western termination of the SEMP Fault (Eastern Alps) and its bearing on the exhumation of the Tauern Window. Geological Society, London, Special Publications 298, 197–218.

Royden, L.H., 1993. Evolution of retreating subduction boundaries formed during continental collision. Tectonics 12, 629–638. doi:10.1029/92TC02641.

Schmid, S.M., Pfiffner, O.A., Froitzheim, N., Schönborn, G., Kissling, E., 1996. Geophysical-geological transect and tectonic evolution of the swiss-italian alps. Tectonics 15, 1036–1064.

Schmid, S.M., Scharf, A., Handy, M.R., Rosenberg, C.L., 2013. The tauern window (eastern alps, Austria): a new tectonic map, with cross-sections and a tectonometamorphic synthesis. Swiss J. Geosci. 106, 1–32. doi:10.1007/s00015-013-0123-y.

Schuster, R., Kurz, W., Krenn, K., Fritz, H., 2013. Introduction to the Geology of the Eastern Alps. Berichte der Geologischen Bundes-Anstalt Wien 99, 121–133.

Schwarz, G., 1978. Estimating the dimension of a model. The annals of statistics , 461–464.

Spada, M., Bianchi, I., Kissling, E., Agostinetti, N.P., Wiemer, S., 2013. Combining controlled-source seismology and receiver function information to derive 3-D Moho topography for Italy. Geophys. J. Int. 194, 1050–1068. doi:10.1093/gji/ggt148.

Stüwe, K., Schuster, R., 2010. Initiation of subduction in the Alps: Continent or ocean? Geology 38, 175–178. doi:10.1130/G30528.1.

Sun, W., Zhao, L., Malusà, M.G., Guillot, S., Fu, L.Y., 2019. 3-D Pn tomography reveals continental subduction at the boundaries of the Adriatic microplate in the absence of a precursor oceanic slab. Earth Planet. Sci. Lett. 510, 131–141. doi:10.1016/j.epsl.2019.01.012.

Tomek, C., Hall, J., 1993. Subducted continental margin imaged in the Carpathians of Czechoslovakia. Geology 21, 535–538. doi:10.1130/0091-7613(1993)021<0535:SCMIIN>2.3.CO;2.

Ustaszewski, K., Schmid, S.M., Fügenschuh, B., Tischler, M., Kissling, E., Spakman, W., 2008. A map-view restoration of the Alpine-Carpathian-Dinaridic system for the Early Miocene. Swiss J. Geosci. 101, 273–294. doi:10.1007/s00015-008-1288-7.

Valasek, P., Mueller, S., Frei, W., Holliger, K., 1991. Results of NFP 20 seismic reflection profiling along the Alpine section of the European Geotraverse (EGT). Geophys. J. Int. 105, 85–102. doi:10.1111/j.1365-246X.1991.tb03446.x.

Vrabec, M., Fodor, L., 2006. Late cenozoic tectonics of slovenia: Structural styles at the northeastern corner of the adriatic microplate, in: Pinter, N., Gyula, G., Weber, J., Stein, S., Medak, D. (Eds.), The Adria Microplate: GPS Geodesy, Tectonics and Hazards, Springer Netherlands, Dordrecht. pp. 151–168. doi:10.1007/1-4020-4235-3_10.

Wölfler, A., Kurz, W., Fritz, H., Stüwe, K., 2011. Lateral extrusion in the Eastern Alps revisited: Refining the model by thermochronological, sedimentary, and seismic data. Tectonics 30. doi:10.1029/2010TC002782.

Yan, Q.Z., Mechie, J., 1989. A fine structural section through the crust and lower lithosphere along the axial region of the Alps. Geophys. J. Int. 98, 465–488. doi:10.1111/j.1365-246X.1989.tb02284.x.

Zahorec, P., Papčo, J., Pašteka, R., Bielik, M., Bonvalot, S., Braitenberg, C., Ebbing, J., Gabriel, G., Gosar, A., Grand, A., Götze, H.J., Hetényi, G., Holzrichter, N., Kissling, E., Marti, U., Meurers, B., Mrlina, J., Nogová, E., Pastorutti, A., Salaun, C., Scarponi, M., Sebera, J., Seoane, L., Skiba, P., Szűcs, E., Varga, M., 2021. The first pan-Alpine surface-gravity database, a modern compilation that crosses frontiers. Earth Syst. Sci. Data 13, 2165–2209. doi:10.5194/essd-13-2165-2021.

Zhao, L., Paul, A., Guillot, S., Solarino, S., Malusà, M.G., Zheng, T., Aubert, C., Salimbeni, S., Dumont, T., Schwartz, S., et al., 2015. First seismic evidence for continental subduction beneath the Western Alps. Geology 43, 815–818. doi:10.1130/G36833.1.

Zhao, L., Paul, A., Malusà, M.G., Xu, X., Zheng, T., Solarino, S., Guillot, S., Schwartz, S., Dumont, T., Salimbeni, S., et al., 2016. Continuity of the Alpine slab unraveled by high-resolution P wave tomography. J. Geophys. Res. Solid 121, 8720–8737.

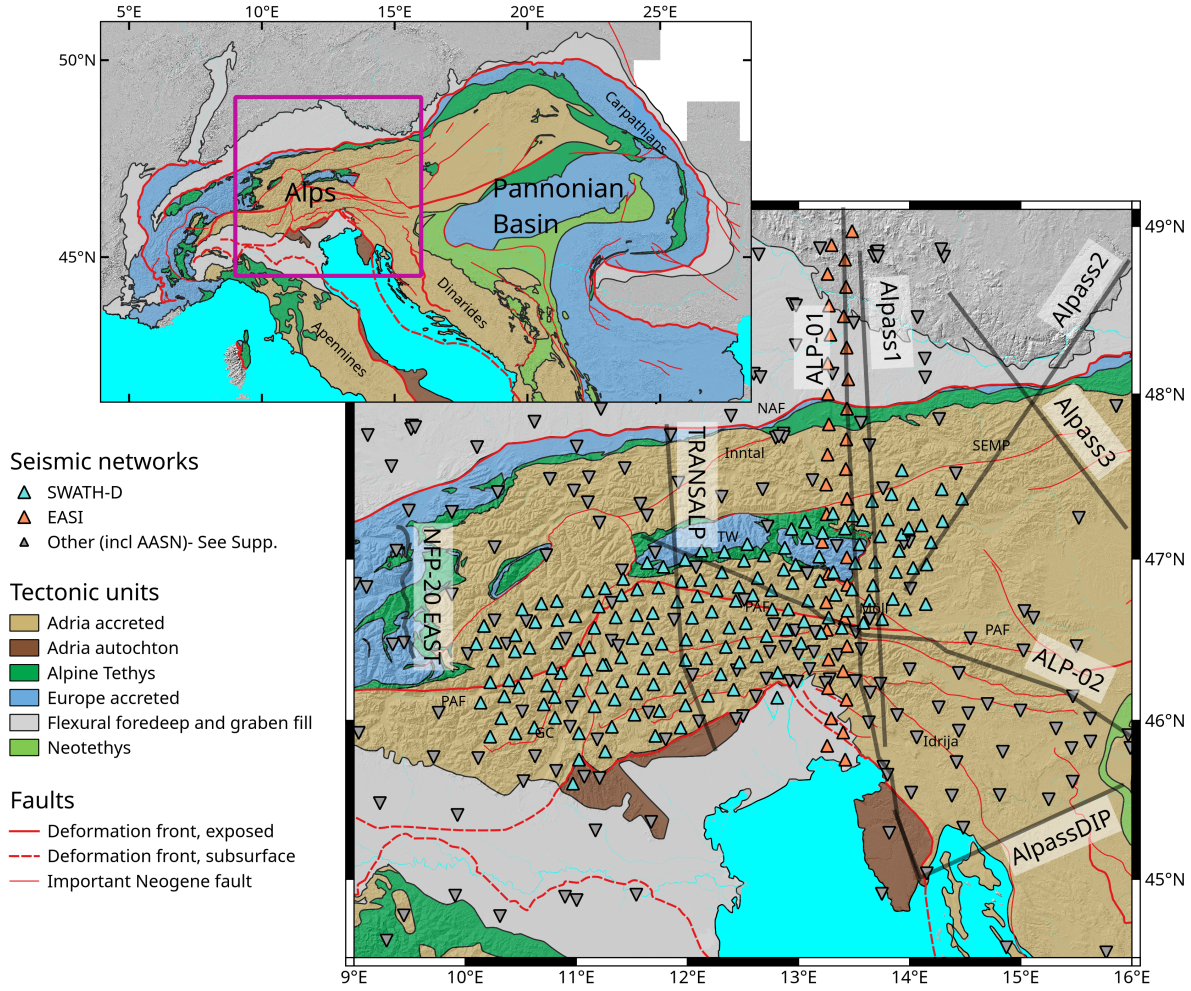

Figure 1: Simplified geological map of the study region with station locations are plotted as triangles. Most stations belong to the dense SWATH-D and EASI deployments, which are supplemented by the temporary AlpArray Seismic Network (AASN) and permanent networks (with full citations in the supplemental material). Controlled source and/or passive seismic lines (NFP-20 East, TRANSALP, ALP-01, ALP-02, Alpass1-3, and AlpassDIP) are shown by grey lines. NAF - Northern Alpine Front, SEMP -Salzach Ennstal Mariazell Puchberg fault, TW - Tauern Window, PAF - Periadriatic Fault, Möll - Mölltal Fault. Tectonic map modified from M.R. Handy based on sources listed in Handy et al. (2019).

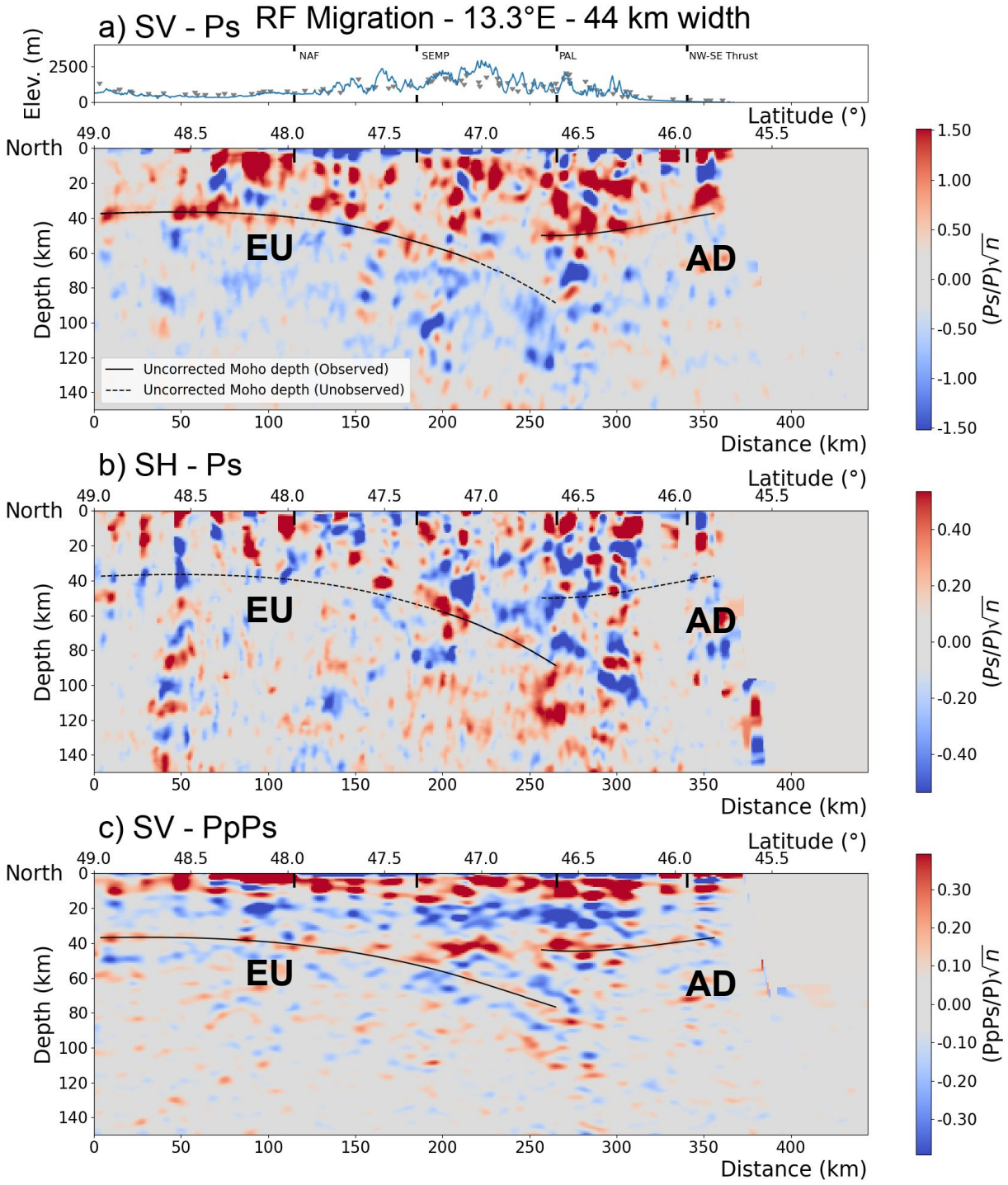

Figure 2: CCP stacks at 13.3°E (longitude of EASI) for the SV (a), SH (b, sensitive to dipping interfaces), and SV PpPs (c, migration for the first multiple) components. The lines show where the Moho interface has been picked. The solid line indicates that an interface was interpreted on that particular stack, while the dashed line indicates that it was picked from another. Traces from events with westerly back-azimuths have had their polarity flipped on the SH component. EU=European Moho and AD=Adriatic Moho.

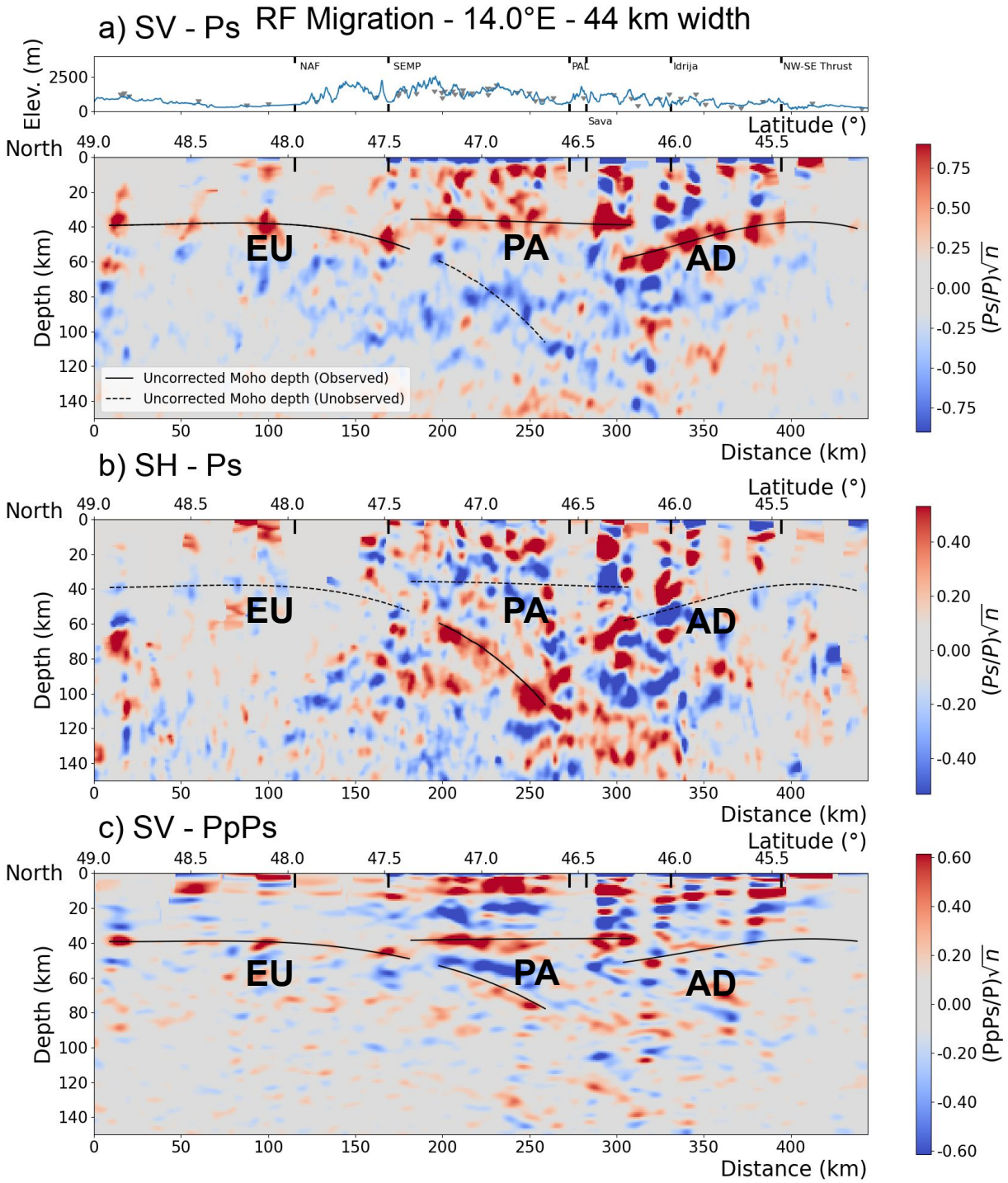

Figure 3: CCP stack at 14°E as in Figure 2.

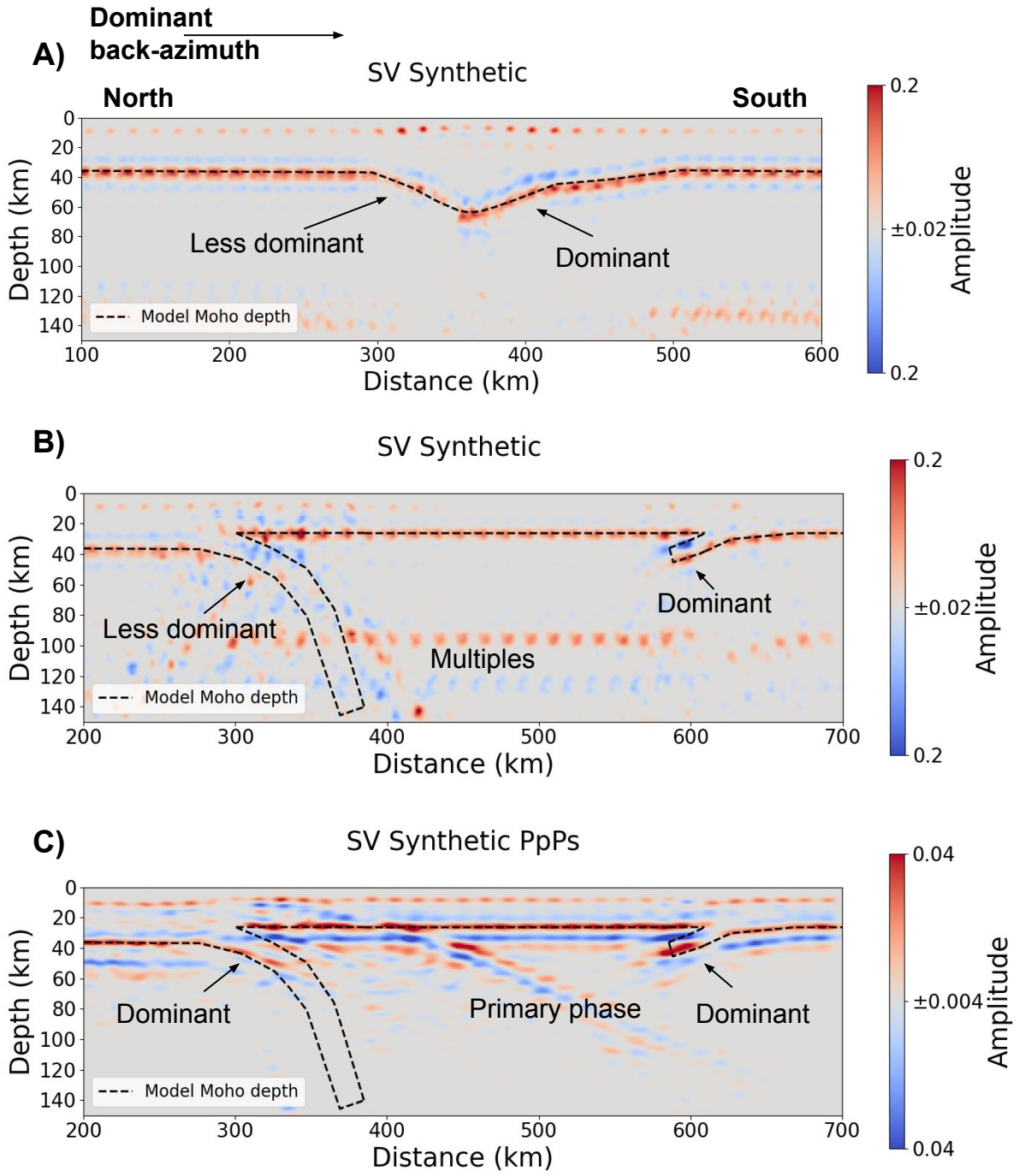

Figure 4: Synthetic 2-layer crust and mantle models with realistic back-azimuthal distribution (assuming N-S orientation with dominant back azimuth from the left/North). **A)** Synthetic trough model, note the dominance for the Moho dipping to the left. **B)** Based on the geometry observed at 14°E. Note the lack of coherent energy from right dipping interfaces. **C)** Same as A but for the first multiple. Note how the initial dipping portion of the Moho can be clearly seen as opposed to in B. Southward dipping phases at 450-600 km are the primary phase migrated upward.

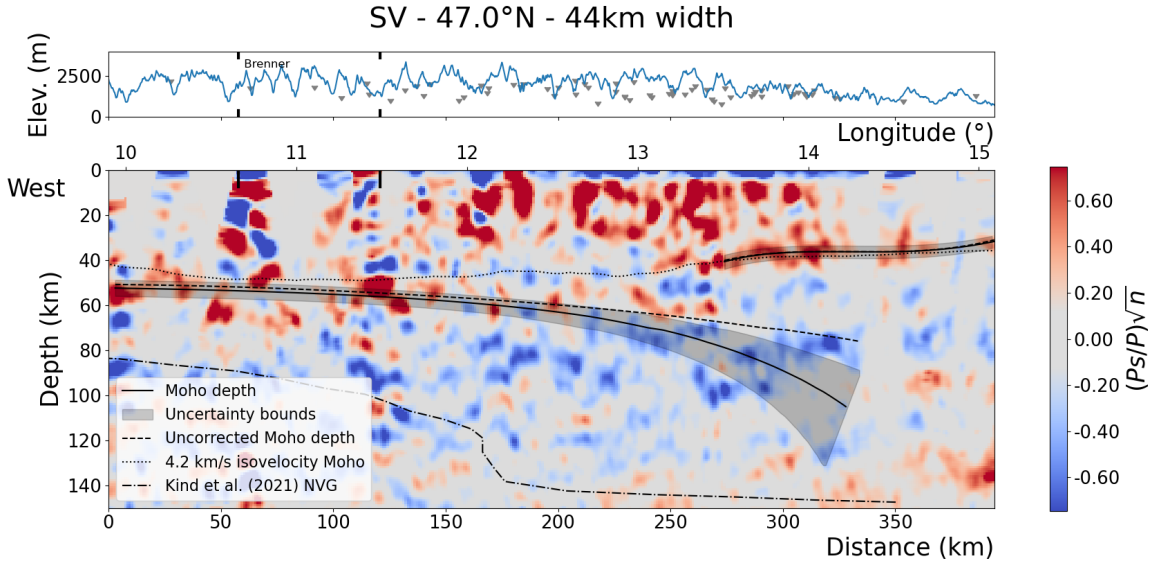

Figure 5: CCP stack for 47.0°N with a swath width of 44 km. At approximately 13.4°E the jump from European to Pannonian Moho can be seen. Note that the marked European Moho beyond this longitude (from ∼13.4°–14.2°) is not visible on the SV component CCP but instead was identified on the North-South SH and SV-PpPs CCP stacks.

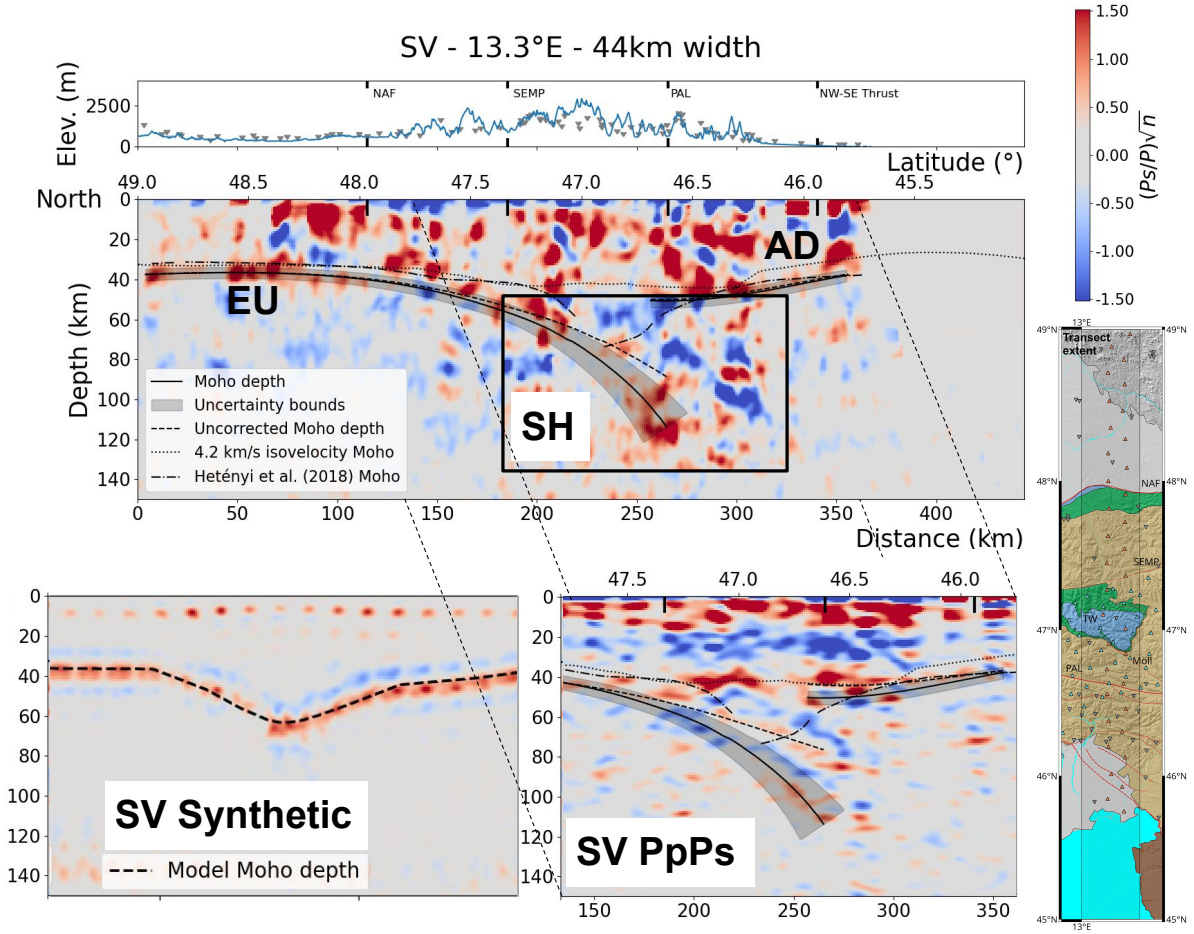

Figure 6: SV CCP stacks for 13.3°E with a swath width of 44 km with the SH component (the polarities of events with back azimuths from the west are flipped) inset and the first multiple (PpPs, below). Both the SH component and the multiple are more sensitive to dipping layers which are not observed on the SV component (Figure 2 shows the unaltered images). Red indicates a velocity increase downwards (e.g. the Moho) and blue a velocity decrease. The SV synthetic illustrates the difficulty of imaging southward dipping interfaces, making northward dipping interfaces more dominant. EU=European Moho and AD=Adriatic Moho.

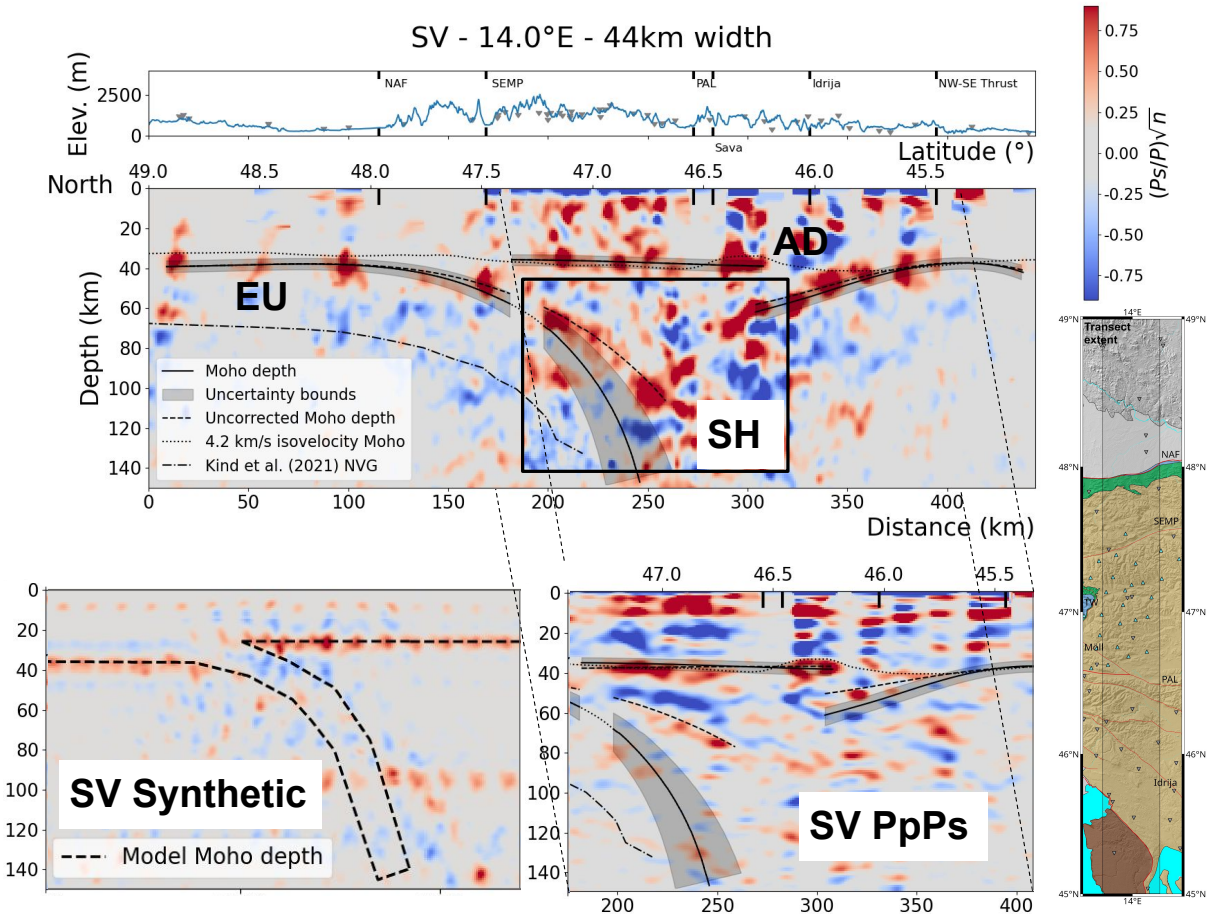

Figure 7: As Figure 6 for the CCP stack at 14°E (unaltered Figure 3). The SV synthetic illustrates why the lack of energy on the true SV component is expected due to a combination of steeply dipping interfaces and lack of illumination from the south. EU=European Moho, AD=Adriatic Moho, and PA=Pannonian Moho.

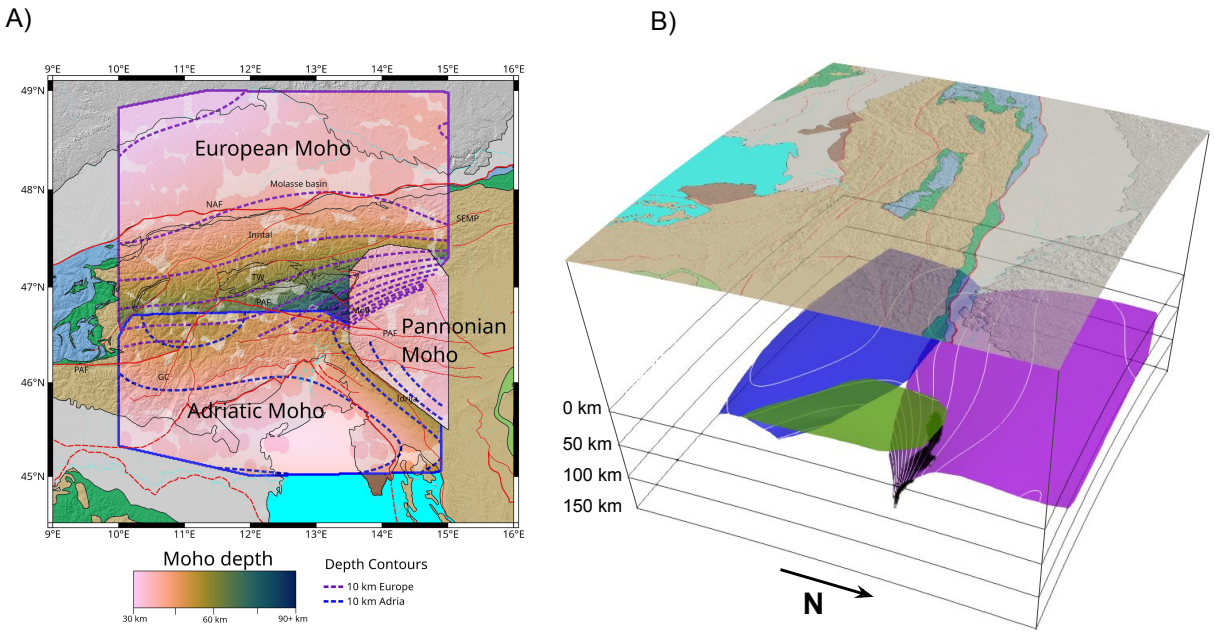

Figure 8: Moho depth map (**A**) showing the three main Moho domains (using the bartlow colour scale (Crameri, 2021)). Paler areas show interpolated depths (no manual picks). The color coded map refers to the shallowest Moho in cases of overlap. Additionally, 10 km contour lines are shown for each domain that highlight the deeper Moho in case of overlaps due to underthrusting. Moving from west to east, the European Moho (purple) underthrusts the shallowly dipping Adriatic Moho (blue). At 13°E, Adriatic Moho begins to retreat southwards into the Dinarides as it underthrusts extended Pannonian crust. Likewise, the European Moho dips steeply beneath the Pannonian Moho (green) to a depth of 150 km. **B**) shows the same Moho geometry in 3-D from northeasterly aspect for the same extent as **A**). Dipping regions of the European Moho where we do not observe energy on either component or the multiples are masked with black

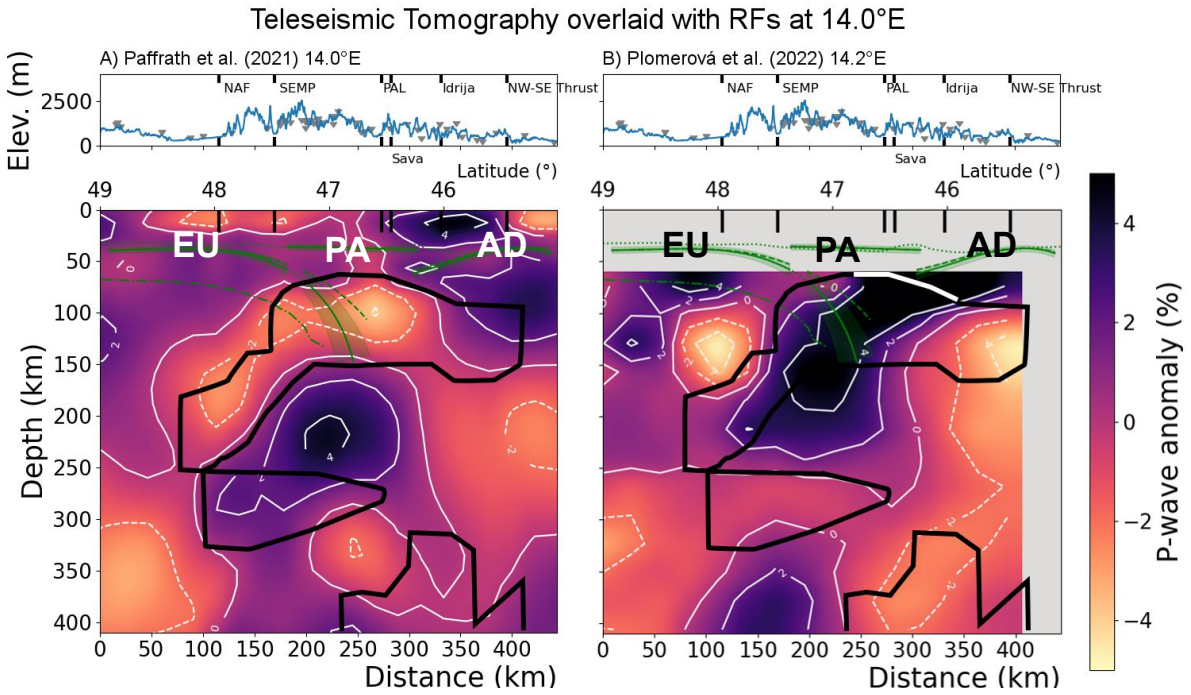

Figure 9: P-wave tomography at 14°E (Paffrath et al., 2021) (**A**) and at 14.2°E (Plomerová et al., 2022) (**B**). The solid black outline shows where the sign of the anomaly is opposite at 14.2°E between the two models. This highlights the central positive slab anomaly or 'consensus slab' which has no clear preferred dip direction. The NVG (lower dot-dashed line) of Kind et al. (2021) (uncorrected for dip/depth) and upper receiver function boundary lead (solid green) into where the consensus slab is located at depth. EU=European Moho, AD=Adriatic Moho, and PA=Pannonian Moho.

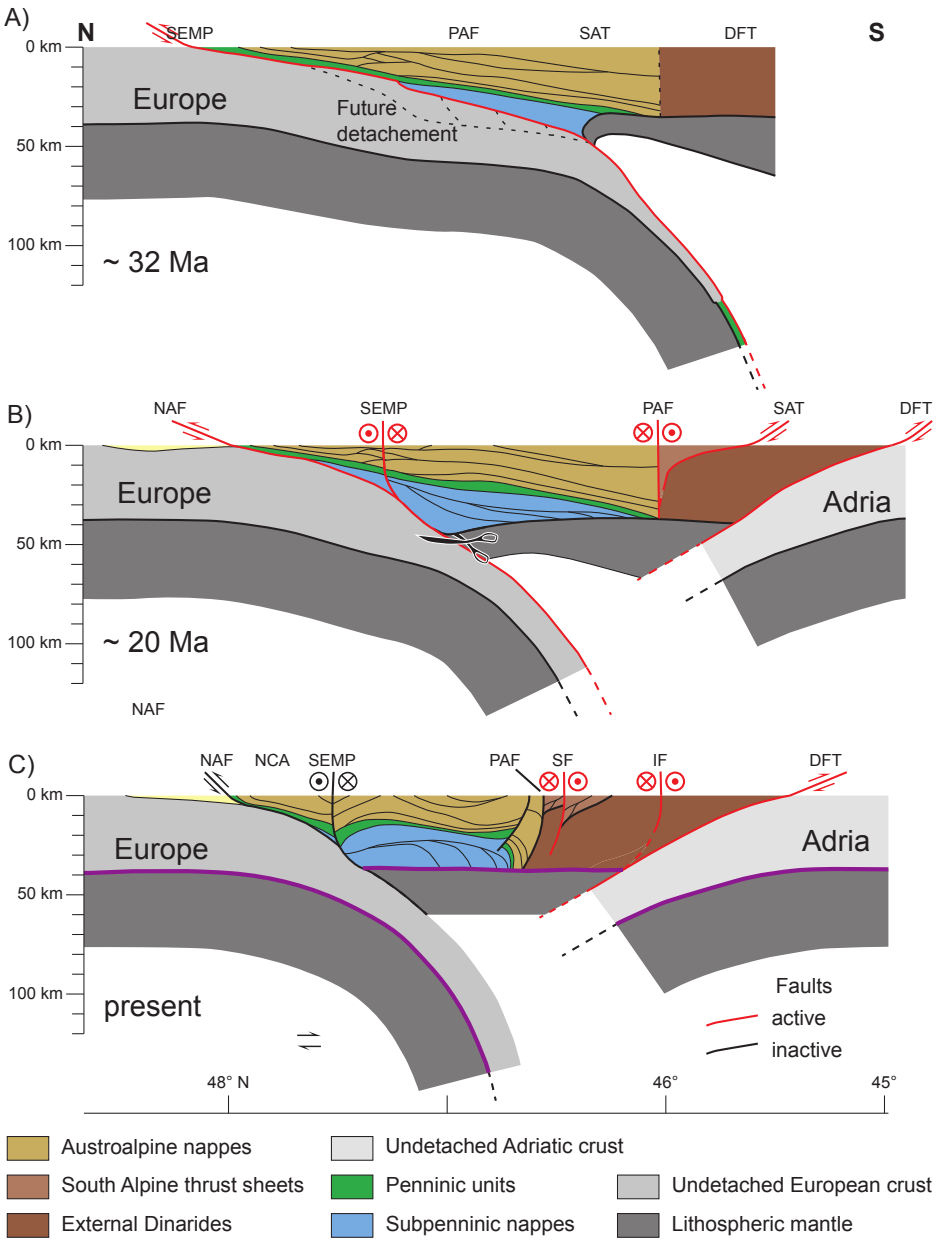
A)
N
S
SEMP
PAF
SAT
DFT
0 km
50 km
100 km
Europe
Future
detachement
~ 32 Ma
B)
NAF
SEMP
PAF
SAT
DFT
0 km
50 km
100 km
Europe
Adria
~ 20 Ma
NAF
C)
NAF
NCA
SEMP
PAF
SF
IF
DFT
0 km
50 km
100 km
Europe
Adria
present
Faults
active
inactive
48° N
46°
45°
Austroalpine nappes
South Alpine thrust sheets
External Dinarides
Undetached Adriatic crust
Penninic units
Subpenninic nappes
Undetached European crust
Lithospheric mantle

Figure 10: Schematic cross sections through the Alps at 14°E illustrating the tectonic evolution of the Pannonian Moho. The restorations are not balanced because of large out-of-plane movements of tectonic units. **A**) Onset of steepening of the European slab after subduction of the Alpine Tethys and distal European margin. Note the presence of a detachment and imbricated structures within the European plate, which will be added to the European accreted units. **B**) Continued steepening of the European slab and onset of eastward escape of the Eastern Alps between the SEMP and Periadriatic Fault led to northward propagation of the Pannonian Moho by insertion of mantle material between the Subpenninic units and undetached European lower crust. Though compared to their present-day geometry, the Eastern Alps were shortened by ~65 km mostly in the Northern Calcareous Alps and just north of the Periadriatic Fault (Linzer et al., 2002), the crust above the Pannonian Moho was not thickened significantly due to the effect of eastward escape. **C**) Present situation, Moho configuration (purple lines) is taken from Figure 7. To the south, the Pannonian Moho extends to below the active Dinaric strike-slip fault system of which only the Idrija fault is shown here. DFT – Dinaric frontal thrust, IF – Idrija Fault, NAF – Northern Alpine Front, NCA – Northern Calcareous Alps, PAF – Periadriatic Fault, SAT – South Alpine frontal thrust, SEMP – Salzach-Ennstal-Mariazell-Puchberg Fault, SF – Sava Fault.